Available online at www.sciencedirect.com
ScienceDirect
Journal of Power Sources 161 (2006) 79–86
JOURNAL OF POWER SOURCES
www.elsevier.com/locate/jpowsour

Effect of metal ion concentration on synthesis and properties of $La_{0.84}Sr_{0.16}MnO_3$ cathode material

A. Kumar, P.S. Devi *, H.S. Maiti

Electroceramics Division, Central Glass and Ceramic Research Institute, Kolkata 700032, India

Received 19 January 2006; accepted 4 April 2006
Available online 7 July 2006

Abstract

A reactive powder of $La_{0.84}Sr_{0.16}MnO_3$ is synthesized as a cathode material for solid oxide fuel cells by a citrate–nitrate auto-ignition process and characterized by thermal analysis, X-ray diffraction and electrical conductivity measurements. The effect of starting metal ion concentration in the precursor solution on the properties of the final oxide is studied and correlated through particle size analyses, sintering studies and microstructural examination. Sintered $La_{0.84}Sr_{0.16}MnO_3$ ceramics of relative density around 93% can be fabricated by preferably keeping the metal ion concentration in the precursor to less than 0.8 M, whereas to make porous ceramics (relative densities of 75–80%) a higher metal ion concentration is preferred. At 1000 °C, the 93% dense ceramics exhibit electrical conductivities of around 168–169 S cm^{-1} and the porous ceramics of around 136–146 S cm^{-1}.

Keywords: Citrate–nitrate; Auto-ignition process; Cathode material; Solid oxide fuel cell; Electrical conductivity; Metal ion concentration

1. Introduction

High-temperature solid oxide fuel cells (SOFCs) are being advanced as power sources with negligible pollution. The units provide many advantages over traditional thermomechanical systems such as high efficiency, reliability, fuel flexibility, a near-zero level of particulate emissions and very low levels of NO_x and SO_x emissions. A SOFC essentially consists of two porous solid electrodes (the cathode and the anode) separated by a dense oxide ion-conducting electrolyte. In the conventional high-temperature SOFC, yttria stabilized zirconia (YSZ) is used as the electrolyte, Ni–YSZ cermet as the anode and Sr-doped lanthanum manganite ($La_{1-x}Sr_xMnO_3$) as the cathode material [1–4].

The perovskite $LaMnO_3$ exhibits p-type conductivity and its electronic conductivity increases by doping with aliovalent ions on either the La or Mn sites. Divalent ions such as Sr, Ca, Ba, Ni or Mg have been incorporated into $LaMnO_3$ lattice [1]. Among the doped manganites investigated, Sr-doped $LaMnO_3$ are the most interesting compounds for SOFC applications. Sr-doping enhances the electronic conductivity of $LaMnO_3$ by the formation of Mn^{4+} for charge compensation as follows:

$$LaMnO_3 \xrightarrow{SrO} La_{1-x}{}^{3+}Sr_x{}^{2+}Mn_{1-x}{}^{3+}Mn_x{}^{4+}O_3 \quad (1)$$

whereas electronic conductivity of $LaMnO_3$ increases with increase in the Sr-doping level, undesirable phase formation usually occurs during processing and fabrication when the Sr-concentration is high. Hence, the Sr-concentration of SOFC cathode materials is usually restricted to 10–20 mol% [1–5]. It has been established by several research groups that among the various Sr-doped $LaMnO_3$ compositions studied, $La_{0.84}Sr_{0.16}MnO_3$ (LSM) – in addition to exhibiting high electronic conductivity – is chemically stable, inert against stabilized zirconia and adheres well to the electrolyte during thermal cycling [1–7]. The electrochemical characteristics of LSM cathode layers depend largely on the microscopic features of the triple-point boundaries (TPB), i.e., the point at which the electrolyte, the cathode and the gas meets, which in turn depend on the starting precursor powder characteristics such as the size, shape and distribution of the constituent particles.

A modified citrate process, known as the *auto-ignition* process, has been developed in our laboratory to prepare multicomponent oxide ceramics that include superconducting oxides and $LaMnO_3$ based oxides [8–12]. This process was later extended for the synthesis and large-scale production of other

* Corresponding author. Tel.: +91 33 2483 8082; fax: +91 33 2473 0957.
E-mail address: psujathadevi@cgcri.res.in (P.S. Devi).

0378-7753/$ – see front matter © 2006 Elsevier B.V. All rights reserved.
doi:10.1016/j.jpowsour.2006.04.122

multi-component oxides [13–15]. Briefly, in this process, a precursor solution consisting of metal nitrates and citric acid was allowed to polymerize completely to form a gel that is then subjected to auto-ignition in the same container to form fine powders. By this process, Sr-doped lanthanum manganite compounds, $La_{1-x}Sr_xMnO_3$, where x varies up to 0.5, were prepared and characterized for SOFC applications [10,11]. Nevertheless, the above studies were performed with keeping a fixed metal ion concentration in the precursor solution. Various other techniques such as, solid state, drip pyrolysis, sol–gel and citrate gel processes are currently available for the preparation of LSM powder samples [6,10–12,16–24]. To our knowledge, there have been no reports of studies of the effect of starting metal ion concentration on the powder characteristics and sintering behaviour of these potentially important oxides. Considering the importance of $La_{0.84}Sr_{0.16}MnO_3$ as a potential cathode material for SOFC fabrication, efforts were undertaken to vary the initial metal ion concentration in the citrate–nitrate precursor solution and to study the effect on the particle size and the sintering characteristics of the derived powders.

2. Experimental

Chemicals: Lanthanum nitrate hexahydrate (Indian Rare Earth Ltd. Mumbai, India 99.9%), strontium nitrate (SD Fine Chem. Ltd., Mumbai, India, 99%), manganese(II) acetate tetrahydrate (E-Merck India Ltd., Mumbai, India, 99.5%) and citric acid monohydrate (Merck Limited, Mumbai, India, 99.5%) were used for sample preparation.

2.1. Synthesis of $La_{0.84}Sr_{0.16}MnO_3$ (hereafter LSM) by citrate–nitrate auto-ignition process

Aqueous solutions of lanthanum nitrate and strontium nitrate were mixed in a stoichiometric ratio of La:Sr = 0.84:0.16 in a 1 l beaker and stirred continuously with a magnetic stirrer. A calculated amount of solid manganese acetate tetrahydrate was added to the mixed solution of metallic (lanthanum and strontium) nitrates to give molar ratio of (La + Sr):Mn equal to unity. To the mixed solution, a calculated amount of citric acid monohydrate was added slowly to maintain a citrate to nitrate ratio (C:N) of 0.75. The mixed solution was allowed to evaporate on a hot plate (200 ± 5 °C) with stirring. When the solution became sufficiently viscous, stirring was stopped but the heating was continued. The homogeneously mixed solution turned into a gel during heating. The gel slowly foamed, swelled and finally burnt on its own. Once ignited at any point, the ignition slowly propagated forward until the whole sample was fully burnt to produce a black coloured powder. This auto-ignition process was completed within a few seconds to a few minutes depending on the starting molar concentration of the metal ions. The product of the auto-ignition process was calcined at elevated temperatures to remove unburnt carbonaceous material and to form a stable mixed-oxide phase. The designations of the various batches prepared and the conditions followed are given in Table 1.

2.2. Physicochemical characterization

Thermogravimetric analysis (TGA) and differential thermal analysis (DTA) of the citrate–nitrate gel were carried out on a NETZSCH STA 409C (Germany) instrument at a heating rate of 20 °C per min. Phase identification of the as-prepared powder and powder calcined at 750 or 900 °C was confirmed from X-ray powder diffraction (XRD) data collected at a scan rate of 2° per min on a Philips PW 3207 (Holland) diffractometer with Cu Kα radiation. The morphology of the synthesized powders was examined by scanning electron microscopy (SEM) using a Leo 430i (UK) scanning electron microscope. The calcined powders (both 750 °C 10 h^{-1} and 900 °C 4 h^{-1}) were ball-milled in an acetone medium for 3.5 h to reduce the particle agglomeration. The particle size was analysed with a Micromerities Sedigraph 5100 unit (U.S.A). The powders were dry-pressed into dimensions of 15 mm × 5 mm × 2 mm at 6.89 MPa pressure using uniaxial pressing. Sintering studies were conducted on these pressed bars within a temperature range of 1200–1350 °C in air for 4 h. The density of the sintered bar was measured by means of the Archimedes principle using white kerosene (density 0.7775 g cm^{-3} at room temperature) as a liquid.

2.3. Electrical characterization

The d.c. electrical conductivity of the highly dense samples was measured up to 1000 °C by a four-probe technique using a HP 3458A multimeter. Electrodes were applied to the samples using pure platinum wire and platinum paste (Gwent Electronics, Pontypool, U.K.).

3. Results and discussion

3.1. Effect of precursor concentration on thermal decomposition characteristics of gel and ash samples

The DTA and TGA of the gel samples of $La_{0.84}Sr_{0.16}MnO_3$ composition prepared from varied metal ion concentrations and

Table 1
Details of different batches of $La_{0.84}Sr_{0.16}MnO_3$

Batch number	Molarity of metal nitrates (La and Sr) used (M)	Total metal ion concentration (M)	Citrate/metal nitrate (C:N) ratio	DTA peak temperature (°C)	Enthalpy change (J g^{-1})
LSM1	0.2	0.40	0.75	186.71	194.57
LSM2	0.5	0.83	0.75	186.12	476.45
LSM3	0.7	1.07	0.75	178.60	286.45
LSM4	1.0	1.33	0.75	136.0	514.47

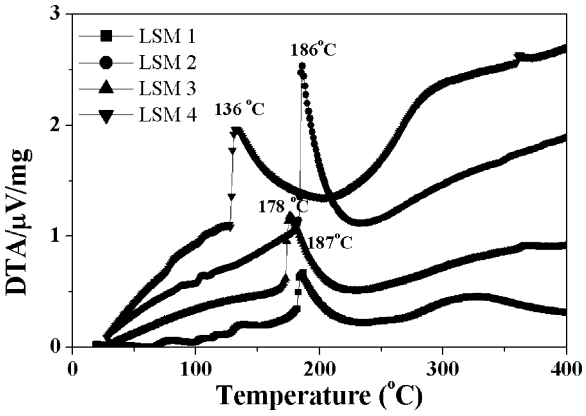

Fig. 1. Differential thermal analysis (DTA) of LSM gel samples.

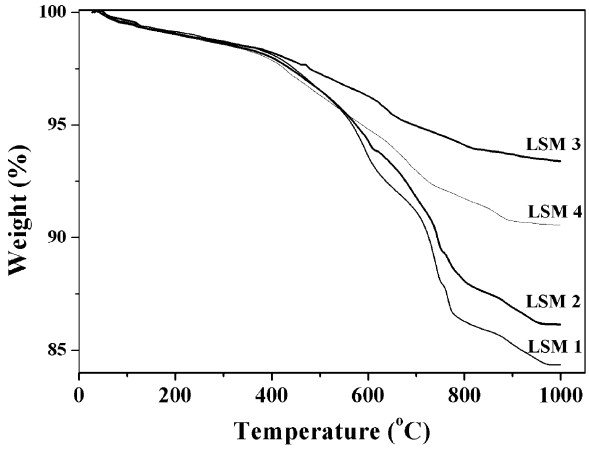

Fig. 3. TGA of as-burnt LSM ash samples.

a fixed C:N ratio of 0.75 are given in Figs. 1 and 2, respectively. Irrespective of the metal ion concentration, all the gel samples exhibit strong exothermic peaks between 135 and 190 °C, which indicates a single-step decomposition of the gels (Fig. 1). The corresponding TGA plots (Fig. 2) are also indicative of a sharp, single-step, decomposition nature. It is evident that the decomposition peak (the peak temperature of ignition) shifts to a lower temperature with increase in the molar concentration of the starting solution. This effect is more apparent at concentrations above 0.8 M. In addition, the burning temperature (ignition temperature) of the gel remains almost same up to a metal ion concentration of 0.83 M, beyond which a decrease in decomposition temperature is observed. The energy change associated with this decomposition reaction increases from 194.57 to 476.45 J g^{-1} for an increase in metal ion concentration from 0.4 to 0.83 M. The enthalpy change does not follow a systematic trend with increase in the metal ion concentration, as revealed by the data given in Table 1. The precursor gel formed from the highly concentrated solution (LSM4), exhibits the highest enthalpy change and the lowest ignition temperature. LSM3 undergoes only a negligible weight loss (1.9%) after the single-step decomposition compared with LSM2 and LSM1 (12.9%). On the other hand, LSM4 shows a 17% weight loss following the single-step decomposition step. This is probably due to the low ignition temperature that is exhibited by the corresponding gel samples. As reported earlier [10–12], this type of a single-step decomposition with a very sharp and intense exotherm indicates a self-propagating combustion process. This can be considered as a thermally induced, anionic redox reaction which occurs within the gel and results in complete decomposition of the organics. So far, the effect of only the citrate to nitrate (C:N) ratio on the auto-ignition reaction has been established for various systems. Through these experiments, it has been found that, in addition to this ratio, the concentration of the cations in the precursor solution play a significant role in controlling the ignition temperature and the enthalpy of the reaction.

The TGA plots of the as-burnt ash samples in air are given in Fig. 3. There is a very slow weight loss up to 400 °C and then a gradual weight loss. This is probably due to the presence of un-burnt carbon and carbonates that have remained in the ash following the auto-ignition reaction. The ash sample of LSM1 suffers the greatest weight loss, viz., around 15%, whereas LSM3 exhibits only 7% weight loss. No definite correlation is observed between the concentration of the metal ions and the weight loss. The observed weight loss within 800–950 °C may be due to the decomposition of unburnt carbonates, the presence of which has yet to be confirmed by XRD. The unexpected decomposition characteristics of the LSM3 sample still require explanation.

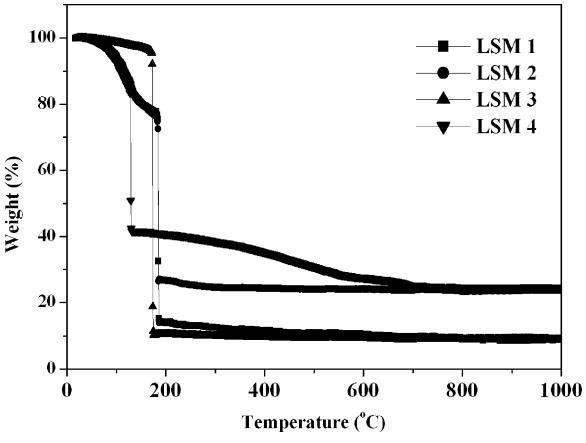

Fig. 2. Thermogravimetric analysis (TGA) data of LSM gels samples.

3.2. *Effect of precursor concentration and temperature on phase formation*

Powder X-ray diffraction data of the as-burnt uncalcined ash samples are presented in Fig. 4. The diffraction data of LSM1 and LSM2 mainly show an amorphous X-ray pattern with indications of the nucleation of a crystalline phase as evident from the presence of a single reflection at around $2\theta = 32.8°$. This reflection corresponds to the ⟨1 1 0⟩ reflection of the perovskite phase. In addition, the presence of minor amounts of $SrCO_3$ is also evident in the XRD patterns of the LSM1 sample. The diffraction data of the LSM3 and LSM4 ash samples, on the other hand, indicate the formation of a single-phase material even in the ash stage itself, with the LSM4 sample displaying all the reflections of a perovskite phase. The direct formation of a perovskite phase

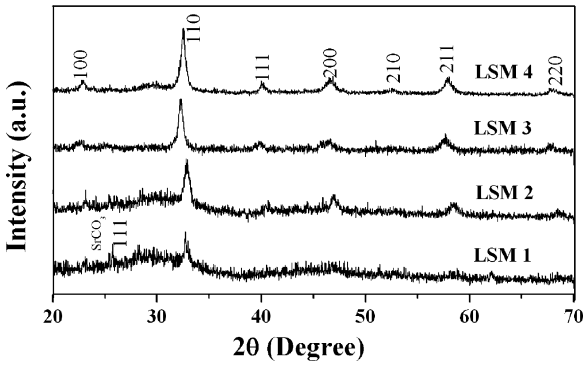

Fig. 4. XRD patterns of as-burnt LSM ash samples.

during the auto-ignition of these gels is in all probability due to the greater extent of compositional homogeneity of the precursor solution and the sufficient amount of in situ heat generated from the exothermic reaction of nitrates and citrates promoting crystallization. It is apparent that due to the intimate contact of the homogeneously distributed metal ions in the gel matrix, the crystalline phase has formed at a considerable rate during the exothermic burning of higher molar concentration gels.

The ash powders were calcined in air at three different temperatures, viz., 750 °C 4 h^{-1}, 750 °C 10 h^{-1} and 900 °C 4 h^{-1}. The diffraction data of the 750 °C 4 h^{-1} calcined sample indicate the formation of pseudo cubic $La_{0.84}Sr_{0.16}MnO_3$ as the major phase with minor amounts of $SrCO_3$ as a secondary phase (Fig. 5). The ⟨1 1 1⟩ and ⟨0 2 1⟩ reflections of $SrCO_3$, which correspond to 100 and 70% intensities, respectively, are clearly seen in the XRD patterns of all the samples. There is a reduction in the intensity of the $SrCO_3$ peak with increase in molar concentration of the starting solution (i.e., from LSM1 to LSM4), which suggests that with increase in the starting precursor concentration more and more strontium ions becomes dissolved in the structure. It may be noted that there were no indications of $SrCO_3$ in the uncalcined ash samples, except for the LSM1 sample. Prolonged heating at 750 °C (10 h) results in the complete removal of $SrCO_3$ peaks, as evident from Fig. 6. A structural change from orthorhombic (pseudo-cubic) to rhombohedral symmetry is evident in the XRD patterns of the 900 °C calcined samples, as indicated by the splitting of the reflections (Fig. 7) in the

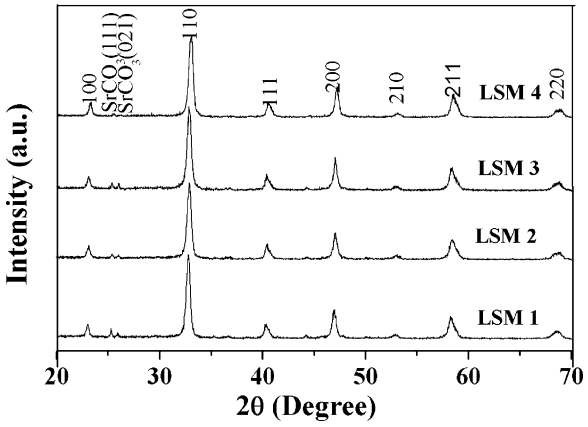

Fig. 5. XRD patterns of 750 °C 4 h^{-1} calcined LSM samples.

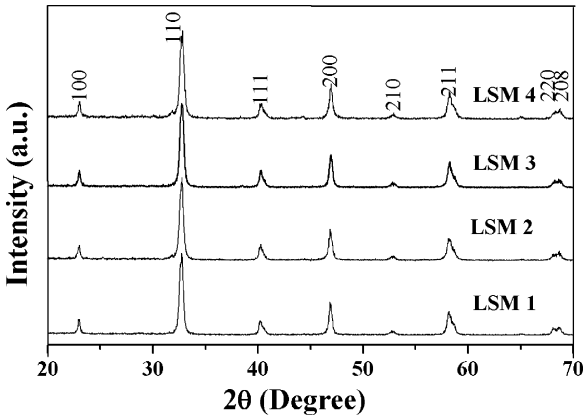

Fig. 6. XRD patterns of 750 °C 10 h^{-1} calcined LSM samples.

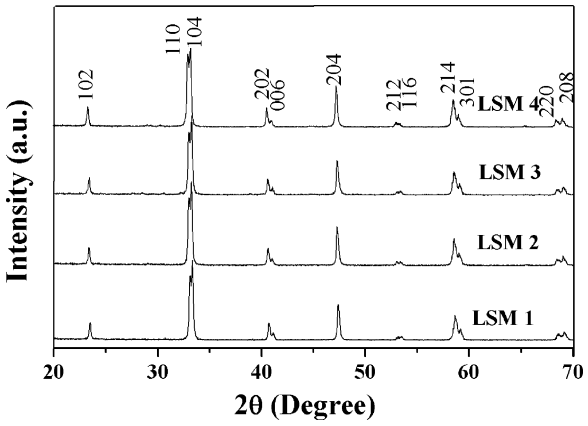

Fig. 7. XRD patterns of 900 °C 4 h^{-1} calcined LSM samples revealing change of symmetry.

XRD pattern. A complete transformation to rhombohedral symmetry is confirmed by the XRD patterns of the 1250 °C sintered samples (Fig. 8).

3.3. Effect of precursor concentration on particle size and distribution

Since the X-ray patterns indicate the formation of fully reacted, single-phase materials both at 750 and 900 °C, the particle size distributions of the 750 °C 10 h^{-1} and 900 °C 4 h^{-1} pow-

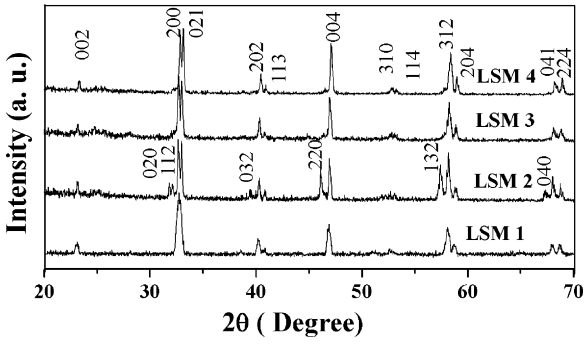

Fig. 8. XRD patterns of 1250 °C 4 h^{-1} sintered LSM samples revealing a complete transformation to rhombohedral symmetry.

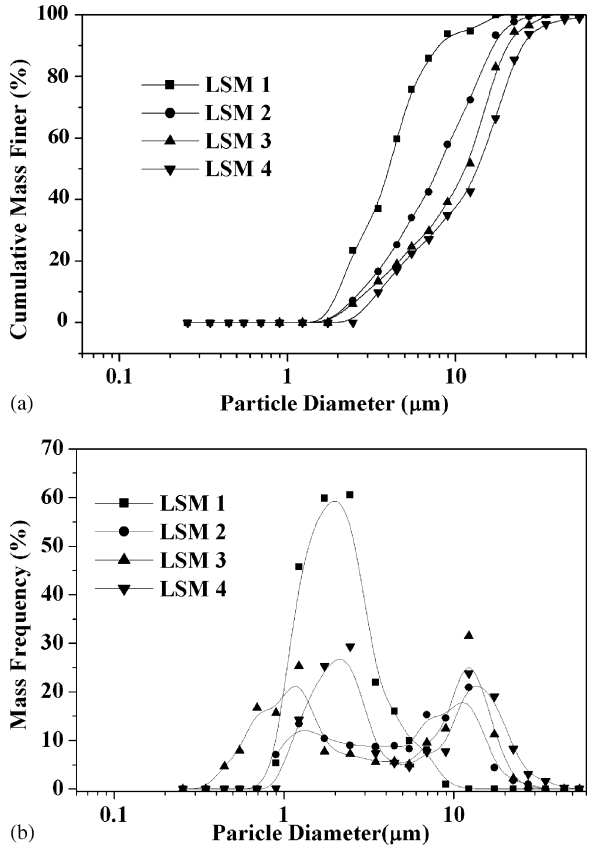

Fig. 9. Particle-size distribution of 750 °C 10 h^{-1} calcined LSM powder samples: (a) percent mass finer distribution; (b) mass frequency distribution.

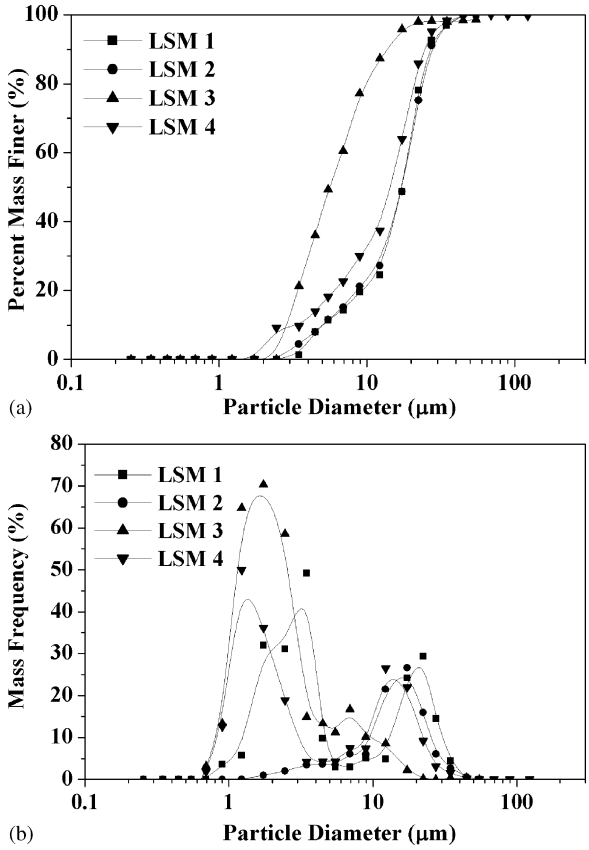

Fig. 10. Particle-size distribution of 900 °C 4 h^{-1} calcined LSM powder samples: (a) percent mass finer distribution; (b) mass frequency distribution.

der samples were compared and are represented in Figs. 9(a) and 10(a), respectively. The corresponding mass frequency graphs are shown in Figs. 9(b) and 10(b). As expected, an increase in particle size (average agglomerate size) with increase in the concentration of the metal ions is evident in the 750 °C 10 h^{-1} calcined samples (Fig. 9(a)). The average agglomerate size increases from 3.98 to 13.74 μm with increase in the metal ion concentration. Except for the LSM1 powder, the others display a bimodal distribution of particles with distinctly separated ranges of particles (Fig. 9b). At higher calcination temperatures, the degree of agglomeration indicates a reverse trend with LSM1 having more agglomeration than the others. The LSM3 sample indicates a decreased particle agglomeration at higher calcination temperature with an average agglomerate size of only 5.7 μm, compared with 17.7 μm for the LSM1 sample (Fig. 10(a)). In addition, LSM3 has a unimodal distribution of particles in contrast to the other samples. SEM micrographs of the 750 °C 10 h^{-1} calcined samples are presented in Fig. 11. The powders are very fine in nature and consist of highly agglomerated particles of 60–120 nm size for LSM1 and LSM2, 100–150 nm for LSM3, and 150–250 nm for LSM4.

3.4. Densification studies of calcined powder samples

A sintering or densification study was carried out on compact green samples in the temperature range 1200–1350 °C. The densification curves of 750 °C 10 h^{-1} and 900 °C 4 h^{-1} calcined samples are given in Figs. 12 and 13, respectively. Irrespective of the calcination temperature, it is found that the powders derived from LSM1 and LSM2 batches are densified to more than 90% at 1350 °C compared with LSM3 and LSM4 samples. In addition, a slow increase in the rate of densification is observed for the LSM1 and LSM2 samples, while a linear change is shown by the LSM3 and LSM4 (Fig. 12). On comparing the percentage densification at 1350 °C of the 750 °C 4 h^{-1} powder samples, a maximum densification of 94.6% is achieved for the LSM1 sample, whereas LSM3 has the lowest density of only 81.3%. The average agglomerate size (d_{50}) and densification (%) at 1350 °C of the different samples are compared in Table 2. It is seen that compacted bars of 750 °C 10 h^{-1} calcined powder are more densified compared with 900 °C 4 h^{-1} calcined samples. This may be due to the increased particle agglomeration and reduced reactivity of the latter samples. These facts clearly suggest that the size and distribution of the particles are important parameters in controlling the densification. Thus, a definite correlation is obtained between the concentration of the precursor solution, the particle size and distribution of the precursor derived powders and the sinterability of the calcined powders.

Electrical and microstructural studies were performed only on the sintered samples derived from the 750 °C 10 h^{-1} calcined powders. The fracture surfaces of the 1350 °C sintered samples developed from these powders are shown in Fig. 14. The sintered ceramic derived from LSM1 shows minimum porosity and the LSM4 has maximum porosity. The LSM1 sample indicates

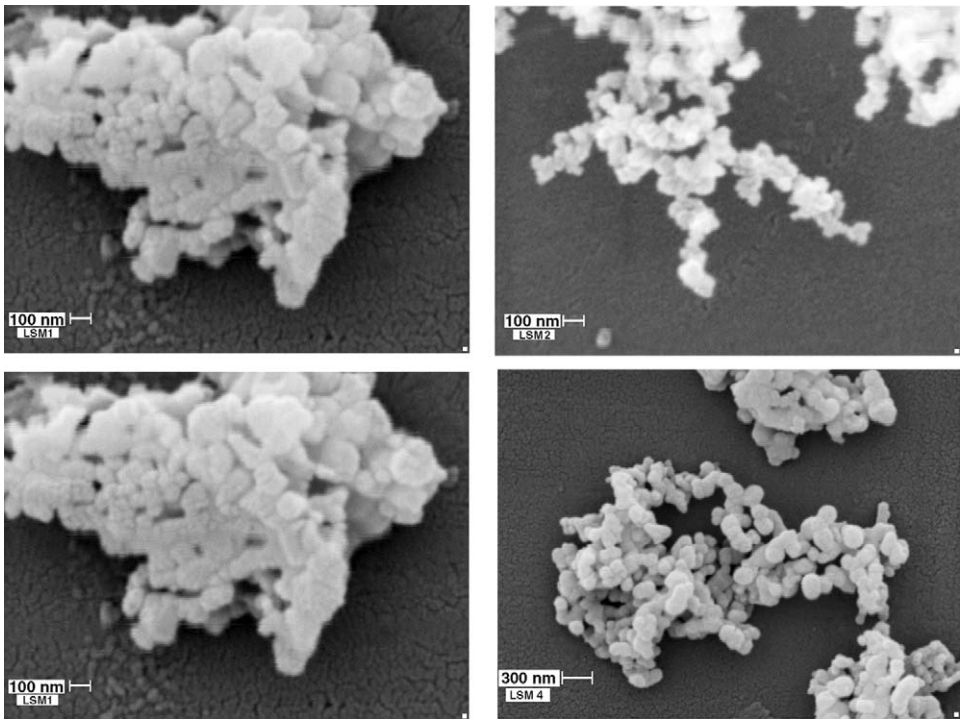

Fig. 11. SEM image of 750 °C 10 h calcined LSM.

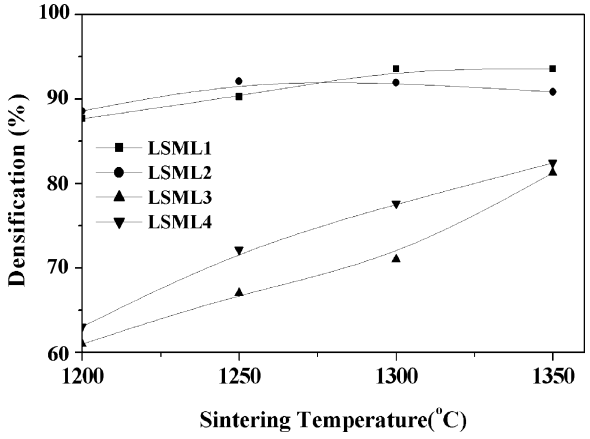

Fig. 12. Densification study of the samples of different batches calcined at 750 °C 4 h^{-1}.

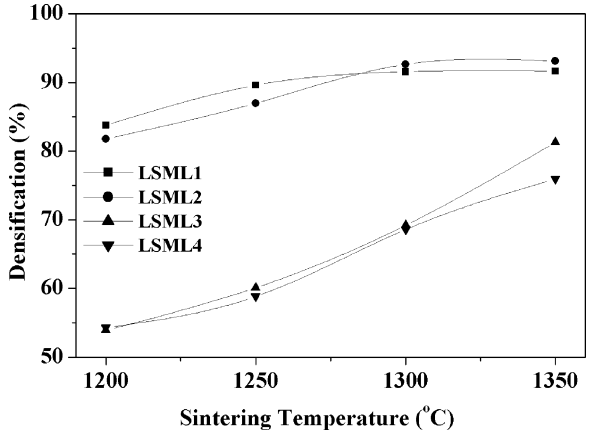

Fig. 13. The densification study of the samples of different batches calcined at 900 °C 4 h^{-1}.

the presence of small intra-grain pores whereas LSM2 contains large intra-grain pores of different size ranges. The high relative densities (93% theoretical density) of LSM1 and LSM2 samples result in a rather small degree of porosity in these samples. It is worth noting the well-connected smaller grains and elongated intra-granular pores present in the LSM3 sample. Heterogeneous pore distribution is more evident for the LSM4 sample as it exhibits both inter-granular and intra-granular pores of different types. This sample consists of relatively dense material and areas containing large voids. A very low relative density (around

Table 2
Comparative data of average particle size and percentage densification of $La_{0.84}Sr_{0.16}MnO_3$

Batch number	Average particle size (d_{50}) (μm)		Percentage densification at 1350 °C	
	750 °C 10 h^{-1} (±0.3)	900 °C 4 h^{-1} (±0.3)	750 °C 10 h^{-1} (±0.3)	900 °C 4 h^{-1} (±0.3)
LSM1	3.98	17.75	94.68	92.66
LSM2	7.84	17.37	93.64	93.11
LSM3	11.35	5.71	81.29	81.27
LSM4	13.74	14.59	82.41	75.96

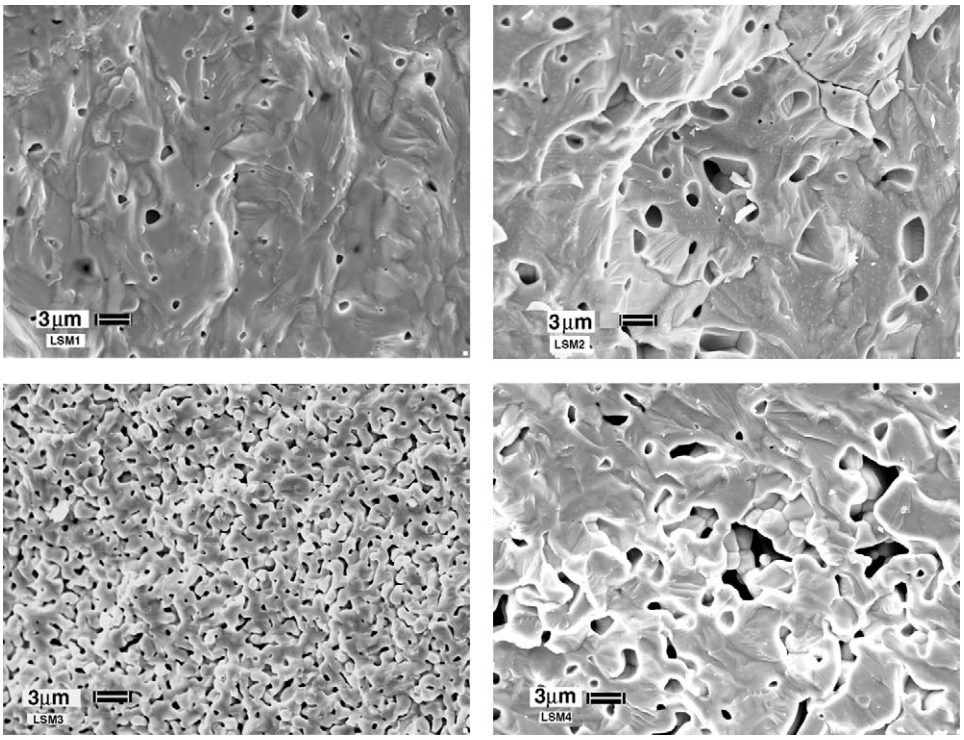

Fig. 14. Microstructure of 1350 °C 4 h^{-1} sintered samples sintered at: (a) LSM1, (b) LSM2, (c) LSM3 and (d) LSM4.

82%) and a highly porous microstructure is characteristic of the LSM3 sample. The microstructure exhibited by LSM3 sintered ceramic sample is that required for SOFC applications.

3.5. Electrical conductivity

Electrical conductivity (σ) measurements were performed on 1350 °C sintered bars derived from 750 °C calcined samples only. The temperature (T) dependence of the electrical conductivity of the 1350 °C sintered samples is shown in Fig. 15. The log (σT) versus 1000/T Arrhenius plot of all the samples exhibit a linear dependence over a wide range of temperature. The slopes of the plots for the LSM1 and LSM2 samples are almost identical, whereas for the other two samples the slopes appear to be similar. It has been reported that such a linear dependence is characteristic of a polaron-hopping transport mechanism [1]. The LSM1 sample exhibited the highest conductivity among the four batches. The activation energy for hopping conduction was calculated from the slopes of the Arrhenius plots and is tabulated in Table 3 along with the conductivity at 1000 °C. The observed activation energy is slightly higher than the value reported for the 1500 °C sintered LSM sample that is around 0.96 eV. The

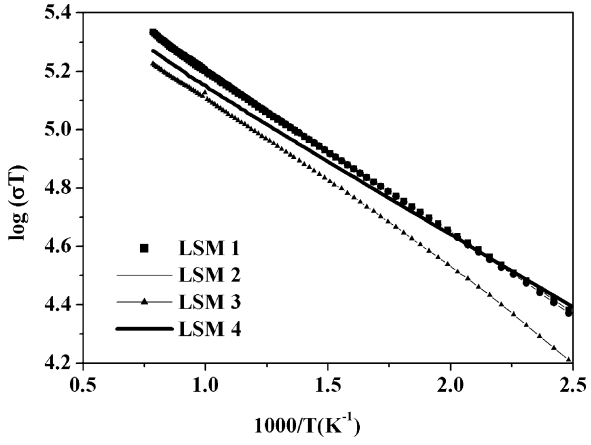

Fig. 15. log(σT) vs. 1000/T plot of sintered LSM samples.

highly sintered samples (LSM1 and LSM2) have a bulk conductivity of around 169 S cm^{-1}, which is very close to what has been reported for $La_{0.84}$ $Sr_{0.16}MnO_3$ sintered ceramics [7]. Although, the sintered ceramics contain pores of different sizes and shapes, a linear change of conductivity with density is observed and this indicates a definite correlation between porosity and conductiv-

Table 3
Conductivity and manganese concentrations of different batches of $La_{0.84}Sr_{0.16}MnO_3$

Batch number	Mn^{4+}/Mn (750 °C 10 h^{-1})	Mn^{4+}/Mn (1350 °C 4 h^{-1})	(σ) at 1000 °C (S cm^{-1})	(σ_{corr}) 1000 °C (S cm^{-1})	Activation energy (eV)
LSM1	43	42	169.55	177.44	0.106
LSM2	43	42	168.84	178.10	0.107
LSM3	42	42	136.93	156.00	0.109
LSM4	42	42	146.43	166.03	0.100

ity. In order to correlate the actual porosity/pore fraction present in the sintered ceramic with the bulk conductivity the following correction was introduced and the corrected conductivity (σ_{corr}) values are given in Table 3 [25].

$$\sigma_{corr} = \sigma_p \left[1 + \frac{f}{(1 + f^{2/3})}\right] \quad (2)$$

where 'σ_p' is the measured conductivity and f represents the pore fraction, which is given by:

$$f = 1 - \frac{dp}{dx} \quad (3)$$

where dp is the measured density and dx is the crystallographic density of LSM (6.571 g cm^{-3}). The difference in the σ_{corr} values for different samples implies that in addition to porosity, there are other factors that control the conductivity of the sintered ceramics.

The amount of Mn^{4+} formed by Sr-substitution is another factor that determines the bulk conductivity in these materials. In order to correlate the conductivity data with the amount of Mn^{4+} formed, Mn estimation was carried out titrimetrically. The ratio of Mn^{4+} to total Mn present is shown in Table 3. The Mn^{4+} content is expected to be lower at higher sintering temperature. Interestingly, the amount of Mn^{4+} is found to be the same and does not vary with either the precursor concentration or the sintering temperature. Thus, the observed variation in conductivity is attributed to the porosity present in the sintered materials and is not related to only the Mn^{4+} concentration. If Mn^{4+} is the sole deciding factor, then the corrected conductivity should have been the same for all the samples irrespective of the porosity present. Again, in spite of having a very close average pore fraction, the σ_{corr} values of the LSM3 and LSM4 samples display a large difference in the conductivity. This difference is attributed to the peculiar microstructure of the LSM3 sintered ceramic, which has a large number of smaller elongated pores compared with the LSM4 sample that has a lower number of larger pores [26,27].

4. Conclusions

The effect of variation of metal ion concentration in the citrate–nitrate precursor solution indicates that up to a metal ion concentration of 0.85, the temperature of decomposition remains almost identical and results in less agglomerated calcined powder samples. The high relative densities (93% theoretical density) of the LSM1 and LSM2 samples result in a rather small degree of porosity. Such powders can be sintered to more than 93% at 1350 °C and have electrical conductivities of around 168 S cm^{-1} at 1000 °C. The relatively high density of the LSM1 and LSM2 samples can be ascribed to the reduced agglomerate size of the 750 °C calcined powder samples. The Mn^{4+} content in all the samples is found to be of the same order. Thus, sintered $La_{0.84}Sr_{0.16}MnO_3$ ceramics of relative density around 93% can be produced by keeping the metal ion concentration in the precursor to less than 0.8 M. To make porous ceramics (relative densities of 75–80%), a higher metal ion concentration of more than 0.8 M is preferred.

Acknowledgements

The authors thank the Director of the Central Glass and Ceramic Research Institute (CG&CRI) for his kind permission to publish this paper. A. Kumar is a Junior Research Fellow (JRF) of the Council of Scientific & Industrial Research, Government of India. Technical support from the X-ray and SEM Divisions of CG & CRI and partial financial support from the Ministry of Non-conventional Energy Sources (MNES), Government of India, are also acknowledged.

References

[1] N.Q. Minh, T. Takahashi, Science and Technology of Ceramic Fuel Cells, Elsevier Science B.V., Netherlands, 1995.
[2] N.Q. Minh, J. Am. Ceram. Soc. 76 (1993) 563.
[3] S.P.S. Badwal, K. Foger, Ceram. Int. 22 (1996) 257.
[4] B. Stambouli, E. Traversa, Renew. Sust. Energy Rev. 6 (2002) 433.
[5] R.M. Ormerod, Chem. Soc. Rev. 32 (2003) 17.
[6] S.P. Jiang, J. Power Sources 124 (2003) 390.
[7] M. Kertesz, I. Riess, D.S. Tannhauser, J. Solid State Chem. 42 (1982) 125.
[8] P.S. Devi, H.S. Maiti, J. Solid State Chem. 109 (1994) 35.
[9] P.S. Devi, H.S. Maiti, J. Mater. Res. 9 (1994) 1357.
[10] A. Chakraborty, P.S. Devi, S. Roy, H.S. Maiti, J. Mater. Res. 9 (1994) 986.
[11] A. Chakraborty, P.S. Devi, H.S. Maiti, Mater. Lett. 20 (1994) 63.
[12] A. Chakraborty, P.S. Devi, H.S. Maiti, J. Mater. Res. 10 (1995) 918.
[13] N. Chakrabarty, H.S. Maiti, J. Mater. Chem. 6 (1996) 1169.
[14] P.S. Devi, Y. Lee, J. Margolis, J.B. Parise, S. Sampath, H. Herman, J.C. Hanson, J. Mater. Res. 17 (2002) 2846.
[15] S. Basu, P.S. Devi, H.S. Maiti, J. Mater. Res. 19 (2004) 3162.
[16] J.H. Choi, J.H. Jang, J.H. Ryu, S.M.M. Oh, J. Power Sources 87 (2000) 92.
[17] R.J. Bell, G.J. Millar, J. Drennan, Solid State Ionics 131 (2000) 211.
[18] F. Licci, G. Turilli, P. Ferro, A. Ciccarone, J. Am. Ceram. Soc. 86 (2003) 413.
[19] H.B. Park, H.J. Kweon, Y.S. Hong, S.J. Kim, K. Kim, J. Mater. Sci. 32 (1997) 57.
[20] X. Pingbo, Z. Weiping, Y. Kuo, J. Long, Z. Weiwei, X. Shangda, J. Alloys Compd. 311 (2000) 90.
[21] D.G. Lamas, A. Caneiro, D. Niebieskikwait, R.D. Sànchez, D. Garcia, J. Magn. Magn. Mater. 241 (2002) 207.
[22] A. Poirson, P. Decorse, G. Caboche, L.C. Dufour, Solid State Ionics 99 (1997) 287.
[23] Q. Ming, D. Nersesyan, J.T. Richardson, D. Luss, J. Mater. Sci. 35 (2000) 3599.
[24] A. Tiwari, K.P. Rajeev, J. Mater. Sci. Lett. 16 (1997) 521.
[25] A.K. Tripathi, H.B. Lal, J. Mater. Sci. 17 (1982) 1595.
[26] J. Mizusaki, S. Tsuchiya, K. Waragai, H. Tagawa, Y. Arai, Y. Kuwayama, J. Am. Ceram. Soc. 79 (1996) 109.
[27] H.J. Juretscheke, R. Landauer, J.A. Swanson, J. Appl. Phys. 27 (1956) 838.